Rare Metal Materials and Engineering
Volume 47, Issue 1, January 2018
Online English edition of the Chinese language journal

Available online at www.sciencedirect.com
ScienceDirect

Cite this article as: Rare Metal Materials and Engineering, 2018, 47(1): 0069-0074.

ARTICLE

Band Gap and Raman Shift of InN Grown on Si (100) by Radio-Frequency Sputtering

Wang Xuewen, Li Tingting, Su Xingxing, Wu Zhaoke, Zhai Chunxue, Hu Feng, Zhang Zhiyong, Zhao Wu

Northwest University, Xi'an 710127, China

Abstract: We have grown the InN films with high orientation and various typical micrographs on Si (100) substrate by radio-frequency (RF) sputtering, with Indium used as Indium target, and Nitrogen as Nitrogen source. The X-ray diffraction (XRD) and X-ray photoelectron spectroscopy (XPS) show that all the diffraction peaks are identified to be associated with the wurtzite phase of InN, with high orientation of (101), (100) and (002). The Scanning Electron Microscope (SEM) and Energy Diffraction Spectrum (EDS) reveal that the high-quality crystal films of InN with various typical microstructures could be deposited, especially the standard of the hexagon at 60 W and 0.4 Pa. We also calculated the stress of InN films in E_2 (High) by Raman spectra with an excitative wave length λ= 633 nm at room temperature. The values of the stress are different due to various microstructures. The A_1 (LO) peaks are lower due to the high mobility. The calculated energies are 1.07, 1.13 and 1.32 eV. The XRD, SEM, XPS, Raman spectra, Hall and UV absorption characterizations demonstrate that we could grow different microstructures of thin films to meet the various requirements of sensors and other devices.

Key words: thin films; crystal growth; magnetron sputtering; stress; energy gap

Al, In and Ga nitrides have attracted more attention due to their high electron drift velocity and small effective mass in recent years. With its wurtzite crystal structure and 0.7 eV direct band gap, Indium nitride (InN) is one of the most important materials in semiconductors[1,2], prompting the extremely rapid development of optoelectronic devices, such as IR-detectors[3], semiconductor quantum dots (QDs)[4], THz emitters, and magnetic field sensors[5]. The InN with nice properties makes it be a competitive candidate for new high-speed devices. It has been fabricated by many techniques, for example, plasma-assisted molecular beam epitaxy (PA-MBE), metal organic chemical vapor deposition (MOCVD), radio-frequency (RF) sputtering, and direct current (DC) sputtering. Compared sputtering methods with PA-MBE and MOCVD methods[6], it is less costly and the size of the deposited thin films can be very large. Y. L. Chung et al. have studied Raman scattering and Rutherford backscattering on InN films grown by PA-MBE in 2011[7], S. Feng also grew the InN nanorods by PA-MBE in 2015[8], J. S. Hwang grew InN on sapphire (0001) substrate using a simple resistive heated MOCVD in 2001[9], and W. C. Ke et al. have grown high density InN/GaN nanodot by pulsed mode MOCVD in 2010[10]. And Porntheeraphat and Nukeaw studied the band gap energy (E_g) of InN thin films grown by RF magnetron sputtering in 2008[10], Hiroyuki Shinoda and Nobuki Mutsukura researched the structural and optical properties of RF sputtered InN in N_2/Ar mixed gases in 2006[11], J. M. Khoshman et al. found that the energy ranged 0.88~4.1 eV of sputtering InN onto different substrates in 2006[12], M. Amirhoseiny et al. fabricated the wurtzite nanocrystalline (101) InN films with RF-sputtering in 2014[13]. However, there is no report preparing different morphologies and orientations InN film by RF-sputtering. In this paper, various topographies were grown under different process conditions of

Received date: January 16, 2017
Foundation item: National Natural Science Foundation of China (61405159, 61076002); Natural Science Foundation of Education Commission of Shaanxi Province (2012JK848)
Corresponding author: Wang Xuewen, Ph. D., Professor, School of Information Science and Technology, Northwest University, Xi'an 710127, P. R. China, Tel: 0086-29-88308119, E-mail: wangxuew@nwu.edu.cn

Copyright © 2018, Northwest Institute for Nonferrous Metal Research. Published by Elsevier BV. All rights reserved.

RF-sputtering technology and the properties were studied.

1 Experiment

All InN films were deposited onto Si (100) substrates by RF magnetron sputtering. The (100) Si substrates were cleaned with ethanol, acetone and de-ionized (DI) water for 3 times before being mounted to the substrate holder in the vacuum chamber. The In metal (99.999%), was used as targets while Ar (99.999%) and N_2 (99.999%) was used as working gases. The substrate temperature of the samples were kept at 600 °C for 60 min under the flow of N_2 (20 mL/min) and Ar (20 mL/min). The samples A and B were grown at the air pressure of 0.6 Pa, while the sample C was deposited at 0.4 Pa. The sputtering power can be adjusted from 60 (samples B and C) to 70 (sample A) W. The structures properties of the samples were obtained by X-ray diffraction (XRD, 6100, SHIMADZU) with Cu Kα radiation. The morphologies and the element compositions of the samples were measured with X-ray photoelectron spectroscopy (XPS, ESCALAB 250 XI),Scanning Electron Microscope and E nergy Diffraction Spectrum (SEM, EDS, Hitacathi S-4800). The stress of film samples were analyzed by the measurement of Raman (WITec, Alpha-500). The carrier concentration and mobility variation were measured through employing Hall system (RH 2035 Hall System, PhysTech Gmbh, Germany). Energy was tested by UV absorption (UV-1800i, SHIMADZU).

2 Results and Discussion

2.1 Crystal structure measurement of the samples

The XRD patterns of thin film samples which grew on the Si (100) substrate at 600 °C with different sputtering powers and air pressures are shown in Fig.1. And the XPS patterns are shown in Fig.2. Sample A was prepared under 0.6 Pa air pressure while the sputtering power was 70 W, Sample B was deposited at 60 W under 0.6 Pa, while sample C was grown at 60 W under 0.4 Pa.

In Fig.1, all the diffraction peaks are identified to be associated with the wurtzite phase of InN (PDF 50-1239)[14]. It can be seen that the InN films are preferentially oriented in different directions. That is in detail, the stronger peak at 33.14° in the sample A, 29.16° in the sample B, and 31.32° in the sample C, which are the diffractions assigned to the (101), (100) and (002) respectively of the wurtzite type InN. All diffraction peaks in the sample A can be indexed to cubic phase and hexagonal InN structure[15]. Another peak at 38.783° is due to the (100) diffraction of Si substrate in the sample B and C of Fig.1. The bigger reflection width (1°) which is FWHM (full width at half maximum) suggests that the grain size belongs to large particles, and the sharpness of the InN spectral is consistent with good crystalline quality. The film preferentially oriented in (101) direction grew on Si (100) at 70 W with 0.6 Pa, and the InN sample B with (100) direction preferentially oriented could be compounded when the sputtering power changed to 60 W, and then the InN sample C would preferentially orient to c-axis (002) when the air pressure decreased from 0.6 to 0.4 Pa.

We used XPS spectra to analyze the surface composition of InN. Each element peak was revised by the C 1s (284.8 eV). From the wide scan XPS spectra, we can see that there are three elements on the surface of InN, In, N, and O in Fig.2. The peaks at the position of 443.8, 451.4, 398.4 eV correspond to In $3d_{5/2}$, In $3d_{3/2}$, N 1s peak, respectively. Compared to the paper reported by Harish Parala, the results of In $3d_{5/2}$ and In $3d_{3/2}$ are almost same[16]. But in the report of Qiang Jing, the two binding energy are high, because of a series of Auger peaks of Indium in the XPS spectra[17]. The binding energy of InN in this paper are basically identical with the standard material. Therefore we can accurately determine the energy loss peak of the most clean samples. For the O elements appearing in InN, we consider it comes from O_2 in the air. Because in a wet environment, O_2 is more easily absorbed on the substrates, so we use XPS spectra to analyse the form of the O element. From the formula:

$$X=\left[A_x/S_x\right]\Big/\sum_{i=1}^{N}A_i/S_i \qquad (1)$$

We can calculate the percentage contents of each elements. Here, X is element percentage. A_x is the area of the peak, and S_x is a sensitivity factor of the element. On the InN surface, In

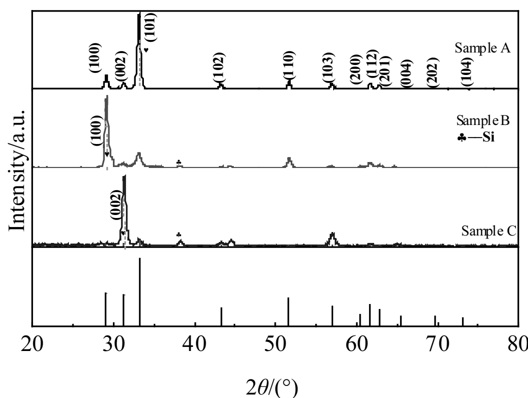

Fig.1 XRD patterns of the InN thin films

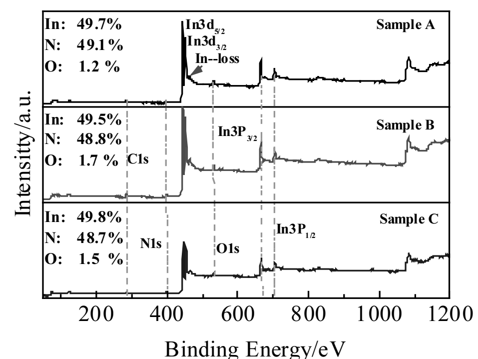

Fig.2 XPS patterns of the InN thin films

and N atomic ratio is about 1:1. It is consistent with the result of EDS shown in Table 1, which further show that the quality of laboratory prepared InN thin film is very high[18].

2.2 Microstructure Analysis of the samples

Fig.3 shows the typical SEM micrographs and the EDS spectrum of the top surface view of InN films which grew on the Si (100) substrate. It can be found that the epitaxy of InN films change as the sputtering powers are decreased from 70 to 60 W, and the pressures are reduced from 0.6 to 0.4 Pa. It can be concluded that the micrograph of sample A is a rectangle, because the sample A was grown in stronger (101) direction in Fig.1, and average size of the gains is about 600 nm. When sample B deposited in (100) direction in Fig.1, the triangular edges can be seen clearly in the Fig.3b, the average size is about 200 nm. The standard hexagon on the top surface is found in Fig.3c due to the orient in the *c*-axis (002), and the average size of the gains is about 150 nm. H. Sugiura et al.[19] have explored the same microtopography result. The size of crystalline grains is expanded (600>200>150 nm) with In and N ions increasing due to the increasing of the power and the pressure. The crystalline grains shown in Fig.3 are various micrographs of typical wurtzite, which mutually corroborate with the result of the reflection widths in Fig.1. It can be found that the surface is very smooth. We hardly find any other impurity elements except Si substrate and O in EDS spectrum and Table 1, which can be seen in Fig.1.

Table 1 shows the percentages of elements in the sample A, B and C. All the samples are slightly In rich. It is clear that the In content increases with the increase of the sputtering power. The rate of In:N:O increases from 1:0.97:0.03 to 1:0.98:0.034 by reducing the air pressure. From this, it can be concluded that the sputtering power and pressure play an important role in depositing InN films. High power is conducive to the reaction of In atom, and lower pressure is beneficial to the synthesis of InN which improve the electrical properties, because the positions of potential minima are occupied by more activation energy with high power[20]. Thus by changing the power and the pressure, high-quality crystal films of InN with various typical micrographs could be deposited. We can find the same results from XPS test.

Table 1 Composition of InN films synthesized on Si (100) substrates

Sample	Element	at%
A	N	49.1
	In	49.7
	O	1.2
B	N	48.8
	In	49.5
	O	1.7
C	N	48.7
	In	49.8
	O	1.5

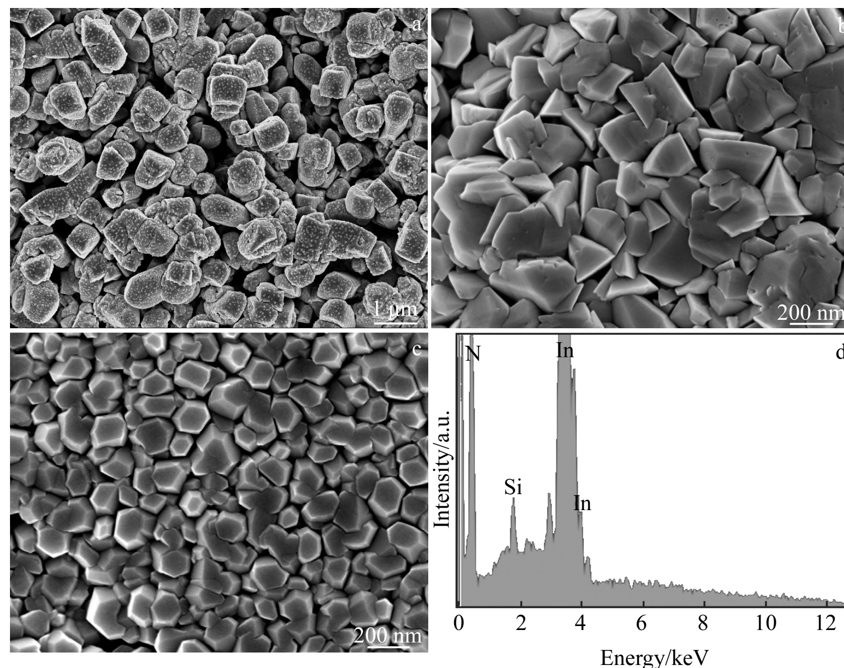

Fig.3 Typical SEM micrographs of InN structures deposited at various powers and air pressures: (a) 70 W, 0.6 Pa, (b) 60 W, 0.6 Pa, and (c) 60 W, 0.4 Pa; (d) EDS spectrum of sample A

2.3 Surface Raman analysis

The Raman spectra of sample A, B, and C with an excitation wavelength λ=633 nm at room temperature are shown in Fig.4. Peaks at 585, 586, and 586 cm^{-1} are assigned to A_1 (LO) of InN films. The E_2 (High) peaks of sample A, B, and C are observed at 490.88, 490, and 492.51 cm^{-1} respectively. The E_2 phonon mode of the InN film in the Raman spectra is affected by the presence of residual stress in the film; hence the strain present in the InN film can be measured[14]. Besides the InN phonon modes, a phonon mode at 520 cm^{-1} from the Si (100) substrate is also observed in the sample A, B, and C. The stresses obtained by the position of E_2 (High) in Fig.4 are determined by the equation that C. Pinquier et al. reported[21,22]. $\Delta\omega=K_b\sigma_b$, where $\Delta\omega$ is the Raman shift in cm^{-1}, K_b = 5.6 and σ_b is the stress expressed in GPa. The InN is freestanding while the E_2 (High) peak position is expected to be at 490 cm^{-1}[23].

Therefore, the values of σ_b are calculated to be +0.16, 0, and +0.44 GPa corresponding to the sample A, B, and C, respectively. That is the sample B which is grown stress-free. The values of σ_b are higher than the reported –0.078 and –0.196 GPa[14], due to the large lattice mismatch and the difference of thermal expansion coefficient between InN films and Si (100) substrates[20]. The sample B is stress-free because the small lattice mismatch between InN films is preferentially oriented with (100) direction in Fig.1 and Si (100) substrates. However, there is a large lattice mismatch between the samples A with (101) direction and C with (002) direction in Fig.1 and Si (100) substrates, leading to the higher values of σ_b than sample B, especially sample C.

2.4 Carrier concentration and mobility variation analysis

As shown in Table 2, the samples of A, B, and C have high electron mobility with weak peaks of A_1 (LO)[14]. Therefore, the technologies provide samples better crystallinity and higher mobility.

Carrier concentration and mobility variation are measured through employing Hall system shown in Table 2.

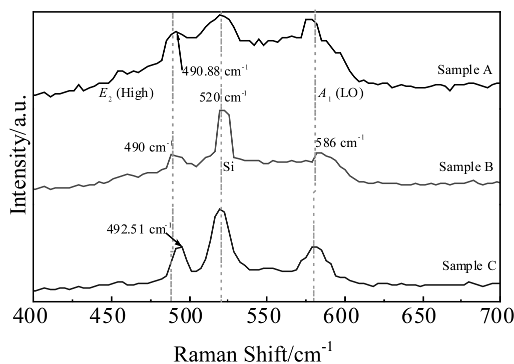

Fig.4 Raman spectra of InN grown on Si (100) of sample A, B, and C with an excitation wavelength λ=633 nm at room temperature

Table 2 Hall tests of samples A, B and C

Sample	Type	Electrical resistivity/Ω·cm	Carrier concentration/cm^{-3}	Mobility/ $cm^2\cdot(V\cdot s)^{-1}$
A	n	1.30×10^3	3.37×10^{17}	197
B	n	2.59×10^2	2.16×10^{18}	223
C	n	1.21×10^3	6.58×10^{17}	201

From Table 2, it can be found that the mobilities of samples A, B and C are 197~223 $cm^2/(V\cdot s)$, which are similar to the report of Barick, B. K[24]. The peak of A_1 (LO) in Fig.3b is lower than that of samples A and B, which suggest that the mobility of sample B is higher than that of A and C. The test of hall shows the same result in Table 2. All type of samples are n, because the films are In rich shown in Table 1. From the results of XRD, SEM, EDS and Raman, impure phases are not found, meaning that the surfaces of samples A, B and C are smoother and the mobility would be increased with the impurities and defects decreasing.

The band gap energy of our samples and some references are presented in Table 3[25]. And the energy curves of InN with different experimental conditions are shown in Fig.5. Compared with those references using the same method, the prepared samples shows lower band gap energy. Because the experiment background vacuum degree is higher, the oxygen content is smaller than the references. From the result of EDS, we can see that the oxygen content of sample A is minimum, so the E_g is the minimum. However, sample B has more oxygen, so its E_g is higher, but less than 2 eV. This phenomenon is close to the result from Davydov et al. who thought the band gap energy is close to 2 eV when oxygen content is close to 20%. The band gap of InN thin film is the smallest, and the crystal quality is the best. V. Y. Davydov et al thought the possible reason for the 1.9 eV band gap is the doping of the impurity oxygen during magnetron sputtering. When the oxygen content was up to 20%, the band gap energy of InN was close to 2 eV[26].

At present, the band gap of InN is 0.9 eV (room temperature), while it is widely believed that the intrinsic band gap of InN was 1.9 eV in the early. In this paper, we can get various band gap of InN under different pressure and power of sputtering by ultraviolet absorption spectrum fitting. The relations between the absorption coefficient and the band gap E_g is:

$$\alpha(h\nu)\propto(h\nu-E_g)^{\frac{1}{2}} \quad (2)$$

Where h is the Planck constant and ν is the incident light

Table 3 UV absorption tests of samples A, B and C

Sample	Sputtering stress/Pa	Sputtering power/W	E_g/eV	$E_{g(Ref.)}$/eV
A	0.6	70	1.07	2.03
B	0.6	60	1.32	2.1
C	0.4	60	1.13	1.97

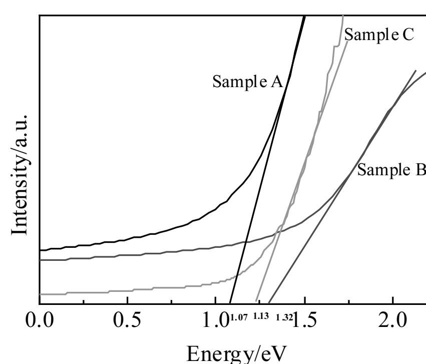

Fig.5 Energy curves of InN with different experimental conditions

frequency[27]. According to the absorption spectrum and this formula, we can get the energy curves in Fig.5. Thus getting the band gap values also means that the value of the optical band gap energy can be approximately determined by the intercept of a linear fit to this curve with the energy axis[28]. The experiment proved that E_g of InN is not only related to the carrier concentration, but also to the pressure and power of the sputtering. The different pressure lead to the average kinetic energy different of films. In Fig.5, we can get the band gap energy of 1.07 and 1.13 and 1.32 eV of InN thin film through different sputtering pressures and power.

Different references of the band gap values of the InN are given in Table 3. Compared with the band gap values in the references, our band gap valueis smaller . While Davydov et al. believed that the entrance of O_2 makes the O atom destroy the In-N key and forms the In_2O_3 which lead to the changing of InN structure; hence the band gap energy of InN thin films are increased[29].

W. Walukiewicz proved that the band gap energy of InN thin films increases as the carrier concentration increases[28], When the carrier concentration is high enough, the bottom of the conduction band will be filled by the carriers. We need more excitation energies than the former band gap if we want to excite the electronics of the valence band to the conduction band which can broaden the optical band gap of film, and give rise to the absorption edge of the film moves towards the short wavelength direction (The increase of the carrier concentration leads to the blue shift of the optical band gap). From this property, we can acquire the continuous tunable direct band gap when we adjust the proportions between the InN and any other group III semiconductor materials, thus developing a photoelectric device in which the photoelectric properties can range from the near infrared to the deep ultraviolet spectrum. The result is consistent with Hall test.

3 Conclusions

1) Changing the power and pressure, we can get different directions of samples.

2) From the SEM micrographs, the standard hexagon can be grown at 0.4 Pa and 60 W, and other typical micrographs can be deposited at 0.6 Pa, which would be available for gas sensor in the future.

3) Raman spectroscopy reveals that the stress-free film can be grown on Si (100) at 60 W with 0.6 Pa, which is helpful to form an air-bridge-like structure with a high aspect ratio[30].

4) The films with lower A_1 (LO) have the high electron mobl ity shown in the Hall test, and the energy of films are less than 1.9 eV which may be available for high-power device.

References

1 Porntheeraphat S, Nukeaw J. *Applied Surface Science*[J], 2008, 254(23): 7851

2 Cai X M, Ye F, Hao Y Q *et al. Journal of Alloys & Compounds* [J], 2009, 484(1-2): 677

3 Amirhoseiny M, Hassan Z, Ng S S *et al. Vacuum*[J], 2014, 106(8): 46

4 Shen C H, Lin H W, Lee H M *et al. Thin Solid Films*[J], 2006, 494(1): 79

5 Ivanov S V, Shubina T V, Komissarova T A *et al. Journal of Crystal Growth*[J], 2014, 403(10): 83

6 Bi Z X, Zhang R, Xie Z L *et al. Journal of Materials Science*[J], 2007, 42(15): 6377

7 Chung Y L, Peng X, Ying C L *et al. Thin Solid Films*[J], 2011, 519(20): 6778

8 Feng S, Tan J, Li B *et al. Journal of Alloys & Compounds*[J], 2015, 621: 232

9 Hwang J S, Lee C H, Yang F H *et al. Materials Chemistry & Physics*[J], 2001, 72(2): 290

10 Ke W C, Lee S J, Kao C Y *et al. Journal of Crystal Growth*[J], 2010, 312(21): 3209

11 Shinoda H, Mutsukura N. *Thin Solid Films*[J], 2006, 503(1-2): 8

12 Khoshman J M, Kordesch M E. *Journal of Non-Crystalline Solids*[J], 2006, 352(52-54): 5572

13 Amirhoseiny M, Hassan Z, Ng S S. *Vacuum*[J], 2014, 101(3): 217

14 Roul B, Rajpalke M K, Bhat T N *et al. Journal of Crystal Growth*[J], 2012, 354(1): 208

15 Yaguchi H, Kitamura Y, Nishida K *et al. Physica Status Solidi*[J], 2005, 2(7): 2267

16 Parala H, Devi A, Hipler F e*t al. Journal of Crystal Growth*[J], 2001, 231(1-2): 68

17 Jing Q, Yang H, Li W *et al. Applied Surface Science*[J], 2015, 331: 248

18 Chauhan A K S, Kumar M, Gupta G. *Applied Surface Science*[J], 2015, 345: 156

19 Sugiura H, Wakasugi S, Mizutani H *et al. Materials Chemistry & Physics*[J], 2008, 108(2): 176

20 Qian Z G, Yu G, Shen W Z *et al. Physica B Condensed Matter*[J], 2002, 318(2-3): 180

21 Wang X, Su X, Hu F *et al. Journal of Alloys & Compounds* [J], 2016, 667: 346

22 Pinquier C, Demangeot F, Frandon J *et al. Phys Rev B*[J], 2004, 70(11): 2516
23 Wang X, Che S B, Ishitani Y *et al. Applied Physics Letters*[J], 2006, 89(89): 171 907
24 Barick B K, Dhar S. *Journal of Crystal Growth*[J], 2015, 416: 154
25 Guo Q X, Tanaka T, Nishio M *et al. Applied Physics Letters*[J], 2005, 86(23): 231 913
26 Davydov V Y, Klochikhin A A, Emtsev V V *et al. Physica Status Solidi*[J], 2002, 234(3): 787
27 Zhao Y, Wu G, Leng J *et al. Vacuum*[J], 2016, 124: 72
28 Schoche S, Hofmann T, Darakchieva V *et al. Journal of Applied Physics*[J], 2013, 113(1): 013 502
29 Sasaoka T, Mori M, Miyazaki T *et al. Journal of Applied Physics*[J], 2010, 108(6): 063 538
30 Vajpeyi A P, Ajagunna A O, Tsiakatouras G *et al. Microelectronic Engineering*[J], 2009, 86(s4-6): 812

采用磁控溅射法在 Si（100）生长 InN 薄膜及其禁带宽度与拉曼的测试

王雪文，李婷婷，苏星星，吴朝科，翟春雪，胡　峰，张志勇，赵　武
(西北大学，陕西 西安 710127)

摘　要：采用磁控溅射法在 Si（100）衬底上生长出高取向性和多种微观形貌的 InN 薄膜，其中铟作为铟靶，氮气作为氮源。X 射线衍射（XRD）和 X 射线光电子能谱（XPS）表明所有衍射峰和标准的纤锌矿晶型的 InN 一致，并且在(101)，(100) 和 (002) 方向具有极高的取向度。扫描电子显微镜(SEM)和能带衍射谱表明，在 Si(100)衬底上可以生长出高质量的不同微观结构的 InN 晶体薄膜，尤其是溅射功率为 60 W，溅射压强为 0.4 Pa 时表现为标准的正六边形结构。在室温下并且激发波长为 λ=633 的拉曼测试表明，可以通过 E_2（High）峰计算出 InN 薄膜的应力，由于微观结构的不同导致应力值也不同，A_1(LO)峰值比较低是由于迁移率较高导致。紫外吸收测试可以计算出的能带宽度分别为 1.07，1.13，1.32 eV。XRD、SEM、XPS、霍尔效应、紫外吸收和拉曼光谱证明生长出的不同微观结构的薄膜可以适应各种需求的传感器和其他设备。

关键词：薄膜；晶体生长；磁控溅射；应力；禁带宽度

作者简介：王雪文，女，1964 年生，博士，教授，西北大学信息科学与技术学院，陕西 西安 710127，电话：029-88308119，E-mail: wangxuew@nwu.edu.cn